



Search for the Higgs boson in $H \rightarrow WW^{(*)}$ decays in $p\bar{p}$ collisions at $\sqrt{s} = 1.96\text{-TEV}$

V.M. Abazov, B. Abbott, M. Abolins, B.S. Acharya, M. Adams, T. Adams,
M. Agelou, J.L. Agram, S.H. Ahn, M. Ahsan, et al.

► To cite this version:

V.M. Abazov, B. Abbott, M. Abolins, B.S. Acharya, M. Adams, et al.. Search for the Higgs boson in $H \rightarrow WW^{(*)}$ decays in $p\bar{p}$ collisions at $\sqrt{s} = 1.96\text{-TEV}$. Physical Review Letters, 2006, 96, pp.011801. 10.1103/PhysRevLett.96.011801 . in2p3-00024523

HAL Id: in2p3-00024523

<https://hal.in2p3.fr/in2p3-00024523>

Submitted on 5 Sep 2023

HAL is a multi-disciplinary open access archive for the deposit and dissemination of scientific research documents, whether they are published or not. The documents may come from teaching and research institutions in France or abroad, or from public or private research centers.

L'archive ouverte pluridisciplinaire **HAL**, est destinée au dépôt et à la diffusion de documents scientifiques de niveau recherche, publiés ou non, émanant des établissements d'enseignement et de recherche français ou étrangers, des laboratoires publics ou privés.

Search for the Higgs boson in $H \rightarrow WW^{(*)}$ decays in $p\bar{p}$ collisions at $\sqrt{s} = 1.96$ TeV

- V.M. Abazov,³⁵ B. Abbott,⁷² M. Abolins,⁶³ B.S. Acharya,²⁹ M. Adams,⁵⁰ T. Adams,⁴⁸ M. Agelou,¹⁸ J.-L. Agram,¹⁹ S.H. Ahn,³¹ M. Ahsan,⁵⁷ G.D. Alexeev,³⁵ G. Alkhazov,³⁹ A. Alton,⁶² G. Alverson,⁶¹ G.A. Alves,² M. Anastasoiae,³⁴ T. Andeen,⁵² S. Anderson,⁴⁴ B. Andrieu,¹⁷ Y. Arnoud,¹⁴ M. Arov,⁵¹ A. Askew,⁴⁸ B. Åsman,⁴⁰ A.C.S. Assis Jesus,³ O. Atramentov,⁵⁵ C. Autermann,²¹ C. Avila,⁸ F. Badaud,¹³ A. Baden,⁵⁹ L. Bagby,⁵¹ B. Baldin,⁴⁹ P.W. Balm,³³ P. Banerjee,²⁹ S. Banerjee,²⁹ E. Barberis,⁶¹ P. Bargassa,⁷⁷ P. Baringer,⁵⁶ C. Barnes,⁴² J. Barreto,² J.F. Bartlett,⁴⁹ U. Bassler,¹⁷ D. Bauer,⁵³ A. Bean,⁵⁶ S. Beauceron,¹⁷ M. Begali,³ M. Begel,⁶⁸ A. Bellavance,⁶⁵ S.B. Beri,²⁷ G. Bernardi,¹⁷ R. Bernhard,^{49,*} I. Bertram,⁴¹ M. Besançon,¹⁸ R. Beuselinck,⁴² V.A. Bezzubov,³⁸ P.C. Bhat,⁴⁹ V. Bhatnagar,²⁷ M. Binder,²⁵ C. Biscarat,⁴¹ K.M. Black,⁶⁰ I. Blackler,⁴² G. Blazey,⁵¹ F. Blekman,⁴² S. Blessing,⁴⁸ D. Bloch,¹⁹ U. Blumenschein,²³ A. Boehlein,⁴⁹ O. Boeriu,⁵⁴ T.A. Bolton,⁵⁷ F. Borcherding,⁴⁹ G. Borissov,⁴¹ K. Bos,³³ T. Bose,⁶⁷ A. Brandt,⁷⁵ R. Brock,⁶³ G. Brooijmans,⁶⁷ A. Bross,⁴⁹ N.J. Buchanan,⁴⁸ D. Buchholz,⁵² M. Buehler,⁵⁰ V. Buescher,²³ S. Burdin,⁴⁹ S. Burke,⁴⁴ T.H. Burnett,⁷⁹ E. Busato,¹⁷ C.P. Buszello,⁴² J.M. Butler,⁶⁰ J. Cammin,⁶⁸ S. Caron,³³ W. Carvalho,³ B.C.K. Casey,⁷⁴ N.M. Cason,⁵⁴ H. Castilla-Valdez,³² S. Chakrabarti,²⁹ D. Chakraborty,⁵¹ K.M. Chan,⁶⁸ A. Chandra,²⁹ D. Chapin,⁷⁴ F. Charles,¹⁹ E. Cheu,⁴⁴ D.K. Cho,⁶⁰ S. Choi,⁴⁷ B. Choudhary,²⁸ T. Christiansen,²⁵ L. Christofek,⁵⁶ D. Claes,⁶⁵ B. Clément,¹⁹ C. Clément,⁴⁰ Y. Coadou,⁵ M. Cooke,⁷⁷ W.E. Cooper,⁴⁹ D. Coppage,⁵⁶ M. Corcoran,⁷⁷ A. Cothenet,¹⁵ M.-C. Cousinou,¹⁵ B. Cox,⁴³ S. Crépé-Renaudin,¹⁴ D. Cutts,⁷⁴ H. da Motta,² M. Das,⁵⁸ B. Davies,⁴¹ G. Davies,⁴² G.A. Davis,⁵² K. De,⁷⁵ P. de Jong,³³ S.J. de Jong,³⁴ E. De La Cruz-Burelo,⁶² C. De Oliveira Martins,³ S. Dean,⁴³ J.D. Degenhardt,⁶² F. Déliot,¹⁸ M. Demarteau,⁴⁹ R. Demina,⁶⁸ P. Demine,¹⁸ D. Denisov,⁴⁹ S.P. Denisov,³⁸ S. Desai,⁶⁹ H.T. Diehl,⁴⁹ M. Diesburg,⁴⁹ M. Dodge,⁴¹ H. Dong,⁶⁹ S. Doulas,⁶¹ L.V. Dudko,³⁷ L. Duflot,¹⁶ S.R. Dugad,²⁹ A. Duperrin,¹⁵ J. Dyer,⁶³ A. Dyshkant,⁵¹ M. Eads,⁶⁵ D. Edmunds,⁶³ T. Edwards,⁴³ J. Ellison,⁴⁷ J. Elmsheuser,²⁵ V.D. Elvira,⁴⁹ S. Eno,⁵⁹ P. Ermolov,³⁷ J. Estrada,⁴⁹ H. Evans,⁶⁷ A. Evdokimov,³⁶ V.N. Evdokimov,³⁸ J. Fast,⁴⁹ S.N. Fataenia,⁶⁰ L. Feligioni,⁶⁰ A.V. Ferapontov,³⁸ T. Ferbel,⁶⁸ F. Fiedler,²⁵ F. Filthaut,³⁴ W. Fisher,⁴⁹ H.E. Fisk,⁴⁹ I. Fleck,²³ M. Fortner,⁵¹ H. Fox,²³ S. Fu,⁴⁹ S. Fuess,⁴⁹ T. Gadfort,⁷⁹ C.F. Galea,³⁴ E. Gallas,⁴⁹ E. Galyaev,⁵⁴ C. Garcia,⁶⁸ A. Garcia-Bellido,⁷⁹ J. Gardner,⁵⁶ V. Gavrilov,³⁶ A. Gay,¹⁹ P. Gay,¹³ D. Gelé,¹⁹ R. Gelhaus,⁴⁷ K. Genser,⁴⁹ C.E. Gerber,⁵⁰ Y. Gershtein,⁴⁸ D. Gillberg,⁵ G. Ginther,⁶⁸ T. Golling,²² N. Gollub,⁴⁰ B. Gómez,⁸ K. Gounder,⁴⁹ A. Goussiou,⁵⁴ P.D. Grannis,⁶⁹ S. Greder,³ H. Greenlee,⁴⁹ Z.D. Greenwood,⁵⁸ E.M. Gregores,⁴ Ph. Gris,¹³ J.-F. Grivaz,¹⁶ S. Grünendahl,⁴⁹ M.W. Grünewald,³⁰ G. Gutierrez,⁴⁹ P. Gutierrez,⁷² A. Haas,⁶⁷ N.J. Hadley,⁵⁹ S. Hagopian,⁴⁸ J. Haley,⁶⁶ I. Hall,⁷² R.E. Hall,⁴⁶ C. Han,⁶² L. Han,⁷ K. Hanagaki,⁴⁹ K. Harder,⁵⁷ A. Harel,²⁶ R. Harrington,⁶¹ J.M. Hauptman,⁵⁵ R. Hauser,⁶³ J. Hays,⁵² T. Hebbeker,²¹ D. Hedin,⁵¹ J.M. Heinmiller,⁵⁰ A.P. Heinson,⁴⁷ U. Heintz,⁶⁰ C. Hensel,⁵⁶ G. Hesketh,⁶¹ M.D. Hildreth,⁵⁴ R. Hirosky,⁷⁸ J.D. Hobbs,⁶⁹ B. Hoeneisen,¹² M. Hohlfeld,²⁴ S.J. Hong,³¹ R. Hooper,⁷⁴ P. Houben,³³ Y. Hu,⁶⁹ J. Huang,⁵³ V. Hynek,⁹ I. Iashvili,⁴⁷ R. Illingworth,⁴⁹ A.S. Ito,⁴⁹ S. Jabeen,⁵⁶ M. Jaffré,¹⁶ S. Jain,⁷² V. Jain,⁷⁰ K. Jakobs,²³ C. Jarvis,⁵⁹ A. Jenkins,⁴² R. Jesik,⁴² K. Johns,⁴⁴ M. Johnson,⁴⁹ A. Jonckheere,⁴⁹ P. Jonsson,⁴² A. Juste,⁴⁹ D. Käfer,²¹ S. Kahn,⁷⁰ E. Kajfasz,¹⁵ A.M. Kalinin,³⁵ J. Kalk,⁶³ D. Karmanov,³⁷ J. Kasper,⁶⁰ I. Katsanos,⁶⁷ D. Kau,⁴⁸ R. Kaur,²⁷ R. Kehoe,⁷⁶ S. Kermiche,¹⁵ S. Kesisoglou,⁷⁴ A. Khanov,⁷³ A. Kharchilava,⁵⁴ Y.M. Kharzeev,³⁵ H. Kim,⁷⁵ T.J. Kim,³¹ B. Klima,⁴⁹ J.M. Kohli,²⁷ J.-P. Konrath,²³ M. Kopal,⁷² V.M. Koralev,³⁸ J. Kotcher,⁷⁰ B. Kothari,⁶⁷ A. Koubarovsky,³⁷ A.V. Kozelov,³⁸ J. Kozminski,⁶³ A. Kryemadhi,⁷⁸ S. Krzywdzinski,⁴⁹ Y. Kulik,⁴⁹ A. Kumar,²⁸ S. Kunori,⁵⁹ A. Kupco,¹¹ T. Kurča,²⁰ J. Kvita,⁹ S. Lager,⁴⁰ N. Lahrichi,¹⁸ G. Landsberg,⁷⁴ J. Lazoflores,⁴⁸ A.-C. Le Bihan,¹⁹ P. Lebrun,²⁰ W.M. Lee,⁴⁸ A. Leflat,³⁷ F. Lehner,^{49,*} C. Leonidopoulos,⁶⁷ V. Lesne,¹³ J. Leveque,⁴⁴ P. Lewis,⁴² J. Li,⁷⁵ Q.Z. Li,⁴⁹ J.G.R. Lima,⁵¹ D. Lincoln,⁴⁹ S.L. Linn,⁴⁸ J. Linnemann,⁶³ V.V. Lipaev,³⁸ R. Lipton,⁴⁹ L. Lobo,⁴² A. Lobodenko,³⁹ M. Lokajicek,¹¹ A. Lounis,¹⁹ P. Love,⁴¹ H.J. Lubatti,⁷⁹ L. Lueking,⁴⁹ M. Lynker,⁵⁴ A.L. Lyon,⁴⁹ A.K.A. Maciel,⁵¹ R.J. Madaras,⁴⁵ P. Mättig,²⁶ C. Magass,²¹ A. Magerkurth,⁶² A.-M. Magnan,¹⁴ N. Makovec,¹⁶ P.K. Mal,²⁹ H.B. Malbouisson,³ S. Malik,⁶⁵ V.L. Malyshev,³⁵ H.S. Mao,⁶ Y. Maravin,⁴⁹ M. Martens,⁴⁹ S.E.K. Mattingly,⁷⁴ R. McCarthy,⁶⁹ R. McCroskey,⁴⁴ D. Meder,²⁴ A. Melnitchouk,⁶⁴ A. Mendes,¹⁵ L. Mendoza,⁸ M. Merkin,³⁷ K.W. Merritt,⁴⁹ A. Meyer,²¹ J. Meyer,²² M. Michaut,¹⁸ H. Miettinen,⁷⁷ J. Mitrevski,⁶⁷ J. Molina,³ N.K. Mondal,²⁹ J. Monk,⁴³ R.W. Moore,⁵ T. Moulik,⁵⁶ G.S. Muanza,²⁰ M. Mulders,⁴⁹ L. Mundim,³ Y.D. Mutaf,⁶⁹ E. Nagy,¹⁵ M. Naimuddin,²⁸ M. Narain,⁶⁰ N.A. Naumann,³⁴ H.A. Neal,⁶² J.P. Negret,⁸ S. Nelson,⁴⁸ P. Neustroev,³⁹ C. Noeding,²³ A. Nomerotski,⁴⁹ S.F. Novaes,⁴ T. Nunnemann,²⁵

E. Nurse,⁴³ V. O'Dell,⁴⁹ D.C. O'Neil,⁵ V. Oguri,³ N. Oliveira,³ N. Oshima,⁴⁹ G.J. Otero y Garzón,⁵⁰ P. Padley,⁷⁷ N. Parashar,⁵⁸ S.K. Park,³¹ J. Parsons,⁶⁷ R. Partridge,⁷⁴ N. Parua,⁶⁹ A. Patwa,⁷⁰ G. Pawloski,⁷⁷ P.M. Perea,⁴⁷ E. Perez,¹⁸ P. Péetroff,¹⁶ M. Petteni,⁴² R. Piegaia,¹ M.-A. Pleier,⁶⁸ P.L.M. Podesta-Lerma,³² V.M. Podstavkov,⁴⁹ Y. Pogorelov,⁵⁴ M.-E. Pol,² A. Pompoš,⁷² B.G. Pope,⁶³ W.L. Prado da Silva,³ H.B. Prosper,⁴⁸ S. Protopopescu,⁷⁰ J. Qian,⁶² A. Quadt,²² B. Quinn,⁶⁴ K.J. Rani,²⁹ K. Ranjan,²⁸ P.A. Rapidis,⁴⁹ P.N. Ratoff,⁴¹ S. Reucroft,⁶¹ M. Rijssenbeek,⁶⁹ I. Ripp-Baudot,¹⁹ F. Rizatdinova,⁷³ S. Robinson,⁴² R.F. Rodrigues,³ C. Royon,¹⁸ P. Rubinov,⁴⁹ R. Ruchti,⁵⁴ V.I. Rud,³⁷ G. Sajot,¹⁴ A. Sánchez-Hernández,³² M.P. Sanders,⁵⁹ A. Santoro,³ G. Savage,⁴⁹ L. Sawyer,⁵⁸ T. Scanlon,⁴² D. Schaile,²⁵ R.D. Schamberger,⁶⁹ Y. Scheglov,³⁹ H. Schellman,⁵² P. Schieferdecker,²⁵ C. Schmitt,²⁶ C. Schwanenberger,²² A. Schwartzman,⁶⁶ R. Schwienhorst,⁶³ S. Sengupta,⁴⁸ H. Severini,⁷² E. Shabalina,⁵⁰ M. Shamim,⁵⁷ V. Shary,¹⁸ A.A. Shchukin,³⁸ W.D. Shephard,⁵⁴ R.K. Shivpuri,²⁸ D. Shpakov,⁶¹ R.A. Sidwell,⁵⁷ V. Simak,¹⁰ V. Sirotenko,⁴⁹ P. Skubic,⁷² P. Slattery,⁶⁸ R.P. Smith,⁴⁹ K. Smolek,¹⁰ G.R. Snow,⁶⁵ J. Snow,⁷¹ S. Snyder,⁷⁰ S. Söldner-Rembold,⁴³ X. Song,⁵¹ L. Sonnenschein,¹⁷ A. Sopczak,⁴¹ M. Sosebee,⁷⁵ K. Soustruznik,⁹ M. Souza,² B. Spurlock,⁷⁵ N.R. Stanton,⁵⁷ J. Stark,¹⁴ J. Steele,⁵⁸ K. Stevenson,⁵³ V. Stolin,³⁶ A. Stone,⁵⁰ D.A. Stoyanova,³⁸ J. Strandberg,⁴⁰ M.A. Strang,⁷⁵ M. Strauss,⁷² R. Ströhmer,²⁵ D. Strom,⁵² M. Strovink,⁴⁵ L. Stutte,⁴⁹ S. Sumowidagdo,⁴⁸ A. Sznajder,³ M. Talby,¹⁵ P. Tamburello,⁴⁴ W. Taylor,⁵ P. Telford,⁴³ J. Temple,⁴⁴ M. Titov,²³ M. Tomoto,⁴⁹ T. Toole,⁵⁹ J. Torborg,⁵⁸ S. Towers,⁶⁹ T. Trefzger,²⁴ S. Trincaz-Duvoud,¹⁷ D. Tsybychev,⁶⁹ B. Tuchming,¹⁸ C. Tully,⁶⁶ A.S. Turcot,⁴³ P.M. Tuts,⁶⁷ L. Uvarov,³⁹ S. Uvarov,³⁹ S. Uzunyan,⁵¹ B. Vachon,⁵ P.J. van den Berg,³³ R. Van Kooten,⁵³ W.M. van Leeuwen,³³ N. Varelas,⁵⁰ E.W. Varnes,⁴⁴ A. Vartapetian,⁷⁵ I.A. Vasilyev,³⁸ M. Vaupel,²⁶ P. Verdier,²⁰ L.S. Vertogradov,³⁵ M. Verzocchi,⁴⁹ F. Villeneuve-Seguier,⁴² J.-R. Vlimant,¹⁷ E. Von Toerne,⁵⁷ M. Vreeswijk,³³ T. Vu Anh,¹⁶ H.D. Wahl,⁴⁸ L. Wang,⁵⁹ J. Warchol,⁵⁴ G. Watts,⁷⁹ M. Wayne,⁵⁴ M. Weber,⁴⁹ H. Weerts,⁶³ N. Wermes,²² M. Wetstein,⁵⁹ A. White,⁷⁵ V. White,⁴⁹ D. Wicke,⁴⁹ D.A. Wijngaarden,³⁴ G.W. Wilson,⁵⁶ S.J. Wimpenny,⁴⁷ M. Wobisch,⁴⁹ J. Womersley,⁴⁹ D.R. Wood,⁶¹ T.R. Wyatt,⁴³ Y. Xie,⁷⁴ Q. Xu,⁶² N. Xuan,⁵⁴ S. Yacoob,⁵² R. Yamada,⁴⁹ M. Yan,⁵⁹ T. Yasuda,⁴⁹ Y.A. Yatsunenko,³⁵ Y. Yen,²⁶ K. Yip,⁷⁰ H.D. Yoo,⁷⁴ S.W. Youn,⁵² J. Yu,⁷⁵ A. Yurkewicz,⁶⁹ A. Zabi,¹⁶ A. Zatserklyaniy,⁵¹ M. Zdrazil,⁶⁹ C. Zeitnitz,²⁴ D. Zhang,⁴⁹ T. Zhao,⁷⁹ Z. Zhao,⁶² B. Zhou,⁶² J. Zhu,⁶⁹ M. Zielinski,⁶⁸ D. Ziemińska,⁵³ A. Ziemiński,⁵³ R. Zitoun,⁶⁹ V. Zutshi,⁵¹ and E.G. Zverev³⁷

(DØ Collaboration)

¹Universidad de Buenos Aires, Buenos Aires, Argentina

²LAFEX, Centro Brasileiro de Pesquisas Físicas, Rio de Janeiro, Brazil

³Universidade do Estado do Rio de Janeiro, Rio de Janeiro, Brazil

⁴Instituto de Física Teórica, Universidade Estadual Paulista, São Paulo, Brazil

⁵University of Alberta, Edmonton, Alberta, Canada, Simon Fraser University, Burnaby, British Columbia, Canada, York University, Toronto, Ontario, Canada, and McGill University, Montreal, Quebec, Canada

⁶Institute of High Energy Physics, Beijing, People's Republic of China

⁷University of Science and Technology of China, Hefei, People's Republic of China

⁸Universidad de los Andes, Bogotá, Colombia

⁹Center for Particle Physics, Charles University, Prague, Czech Republic

¹⁰Czech Technical University, Prague, Czech Republic

¹¹Center for Particle Physics, Institute of Physics, Academy of Sciences of the Czech Republic, Prague, Czech Republic

¹²Universidad San Francisco de Quito, Quito, Ecuador

¹³Laboratoire de Physique Corpusculaire, IN2P3-CNRS, Université Blaise Pascal, Clermont-Ferrand, France

¹⁴Laboratoire de Physique Subatomique et de Cosmologie, IN2P3-CNRS, Université de Grenoble 1, Grenoble, France

¹⁵CPPM, IN2P3-CNRS, Université de la Méditerranée, Marseille, France

¹⁶IN2P3-CNRS, Laboratoire de l'Accélérateur Linéaire, Orsay, France

¹⁷LPNHE, IN2P3-CNRS, Universités Paris VI and VII, Paris, France

¹⁸DAPNIA/Service de Physique des Particules, CEA, Saclay, France

¹⁹IReS, IN2P3-CNRS, Université Louis Pasteur, Strasbourg, France, and Université de Haute Alsace, Mulhouse, France

²⁰Institut de Physique Nucléaire de Lyon, IN2P3-CNRS, Université Claude Bernard, Villeurbanne, France

²¹III. Physikalisches Institut A, RWTH Aachen, Aachen, Germany

²²Physikalisches Institut, Universität Bonn, Bonn, Germany

²³Physikalisches Institut, Universität Freiburg, Freiburg, Germany

²⁴Institut für Physik, Universität Mainz, Mainz, Germany

²⁵Ludwig-Maximilians-Universität München, München, Germany

²⁶Fachbereich Physik, University of Wuppertal, Wuppertal, Germany

²⁷Panjab University, Chandigarh, India

²⁸Delhi University, Delhi, India

²⁹Tata Institute of Fundamental Research, Mumbai, India

³⁰University College Dublin, Dublin, Ireland

- ³¹Korea Detector Laboratory, Korea University, Seoul, Korea
³²CINVESTAV, Mexico City, Mexico
³³FOM-Institute NIKHEF and University of Amsterdam/NIKHEF, Amsterdam, The Netherlands
³⁴Radboud University Nijmegen/NIKHEF, Nijmegen, The Netherlands
³⁵Joint Institute for Nuclear Research, Dubna, Russia
³⁶Institute for Theoretical and Experimental Physics, Moscow, Russia
³⁷Moscow State University, Moscow, Russia
³⁸Institute for High Energy Physics, Protvino, Russia
³⁹Petersburg Nuclear Physics Institute, St. Petersburg, Russia
⁴⁰Lund University, Lund, Sweden, Royal Institute of Technology and Stockholm University, Stockholm, Sweden, and Uppsala University, Uppsala, Sweden
⁴¹Lancaster University, Lancaster, United Kingdom
⁴²Imperial College, London, United Kingdom
⁴³University of Manchester, Manchester, United Kingdom
⁴⁴University of Arizona, Tucson, Arizona 85721, USA
⁴⁵Lawrence Berkeley National Laboratory and University of California, Berkeley, California 94720, USA
⁴⁶California State University, Fresno, California 93740, USA
⁴⁷University of California, Riverside, California 92521, USA
⁴⁸Florida State University, Tallahassee, Florida 32306, USA
⁴⁹Fermi National Accelerator Laboratory, Batavia, Illinois 60510, USA
⁵⁰University of Illinois at Chicago, Chicago, Illinois 60607, USA
⁵¹Northern Illinois University, DeKalb, Illinois 60115, USA
⁵²Northwestern University, Evanston, Illinois 60208, USA
⁵³Indiana University, Bloomington, Indiana 47405, USA
⁵⁴University of Notre Dame, Notre Dame, Indiana 46556, USA
⁵⁵Iowa State University, Ames, Iowa 50011, USA
⁵⁶University of Kansas, Lawrence, Kansas 66045, USA
⁵⁷Kansas State University, Manhattan, Kansas 66506, USA
⁵⁸Louisiana Tech University, Ruston, Louisiana 71272, USA
⁵⁹University of Maryland, College Park, Maryland 20742, USA
⁶⁰Boston University, Boston, Massachusetts 02215, USA
⁶¹Northeastern University, Boston, Massachusetts 02115, USA
⁶²University of Michigan, Ann Arbor, Michigan 48109, USA
⁶³Michigan State University, East Lansing, Michigan 48824, USA
⁶⁴University of Mississippi, University, Mississippi 38677, USA
⁶⁵University of Nebraska, Lincoln, Nebraska 68588, USA
⁶⁶Princeton University, Princeton, New Jersey 08544, USA
⁶⁷Columbia University, New York, New York 10027, USA
⁶⁸University of Rochester, Rochester, New York 14627, USA
⁶⁹State University of New York, Stony Brook, New York 11794, USA
⁷⁰Brookhaven National Laboratory, Upton, New York 11973, USA
⁷¹Langston University, Langston, Oklahoma 73050, USA
⁷²University of Oklahoma, Norman, Oklahoma 73019, USA
⁷³Oklahoma State University, Stillwater, Oklahoma 74078, USA
⁷⁴Brown University, Providence, Rhode Island 02912, USA
⁷⁵University of Texas, Arlington, Texas 76019, USA
⁷⁶Southern Methodist University, Dallas, Texas 75275, USA
⁷⁷Rice University, Houston, Texas 77005, USA
⁷⁸University of Virginia, Charlottesville, Virginia 22901, USA
⁷⁹University of Washington, Seattle, Washington 98195, USA

(Dated: August 27, 2005)

We present a search for the standard model Higgs boson in $H \rightarrow WW^{(*)}$ decays with e^+e^- , $e^\pm\mu^\mp$ and $\mu^+\mu^-$ final states in $p\bar{p}$ collisions at a center-of-mass energy of $\sqrt{s} = 1.96$ TeV. The data, collected from April 2002 to June 2004 with the DØ detector, correspond to an integrated luminosity of $300 - 325 \text{ pb}^{-1}$, depending on the final state. The number of events observed is consistent with the expectation from backgrounds. Limits from the combination of all three channels on the Higgs production cross section times branching ratio $\sigma \times BR(H \rightarrow WW^{(*)})$ are presented.

PACS numbers: 13.85.Rm, 14.80.Bn

In the standard model (SM), the hypothetical Higgs boson is crucial to the understanding of electroweak sym-

metry breaking (EWSB) and the mass generation of electroweak gauge bosons and fermions. Spontaneous EWSB predicts the existence of this neutral scalar particle with mass M_H , a free parameter in the SM. Direct searches at the CERN e^+e^- collider (LEP) yield a lower limit for the Higgs boson mass of $M_H > 114.4$ GeV [1] at the 95% CL. Indirect measurements via fits to the electroweak precision data give an upper bound of $M_H < 280$ GeV [2] at the 95% CL.

In this Letter, we present a search for the Higgs boson in $H \rightarrow WW^{(*)} \rightarrow \ell\nu\ell'\nu'$ ($\ell, \ell' = e, \mu, \tau$) decays with e^+e^- , $e^\pm\mu^\mp$, or $\mu^+\mu^-$ final states. Tau decays are detected in their leptonic decay modes to electrons or muons. This is the first search for the Higgs boson at a hadron collider in this decay channel, which plays an important role in the overall discovery potential of the Higgs boson at the Fermilab Tevatron Collider [3]. We use data collected by the DØ detector between April 2002 and June 2004 in $p\bar{p}$ collisions at $\sqrt{s} = 1.96$ TeV of the Fermilab Tevatron Collider. The integrated luminosities are 325 ± 21 pb $^{-1}$, 318 ± 21 pb $^{-1}$ and 299 ± 19 pb $^{-1}$ for the e^+e^- , $e^\pm\mu^\mp$ and $\mu^+\mu^-$ channels, respectively. The differences in the integrated luminosities for various channels are primarily due to different trigger conditions. Next-to-leading order (NLO) calculations [4, 5] predict the product of the SM Higgs boson production cross section and the branching ratio $\sigma(p\bar{p} \rightarrow H) \times BR(H \rightarrow WW^{(*)})$ of 11–250 fb for the Higgs masses between 100 and 200 GeV. The dominant contribution to the cross section comes from gluon-gluon fusion. Extensions of the SM including a fourth fermion family [6] predict an enhanced Higgs boson production cross section.

We briefly describe the main components of the DØ Run II detector [7] important to this analysis. The central tracking system consists of a silicon microstrip tracker (SMT) and a central fiber tracker (CFT), both located within a 2.0 T axial magnetic field. The SMT strips have a typical pitch of 50–80 μm , and the design is optimized for tracking and vertexing over the pseudorapidity range $|\eta| < 3$, where $\eta = -\ln(\tan \frac{\theta}{2})$, where θ is the polar angle with respect to the proton beam. The system has a six-barrel longitudinal structure, each with a set of four silicon layers arranged axially around the beam pipe, interspersed with sixteen radial disks. The CFT with full coverage for $|\eta| < 1.6$ has eight thin coaxial barrels, each supporting two doublets of overlapping scintillating fibers, one doublet parallel to the beam axis, the other alternating by $\pm 3^\circ$ relative to the beam axis.

A liquid-argon/uranium calorimeter surrounds the central tracking system and consists of a central calorimeter (CC) covering to $|\eta| \approx 1.1$, and two end cap calorimeters (EC) extending coverage to $|\eta| < 4.2$, all housed in separate cryostats [8]. Scintillators between the CC and EC cryostats provide additional sampling of showers for $1.1 < |\eta| < 1.4$.

The muon system is located outside the calorimeters

and consists of a layer of tracking detectors and scintillation trigger counters inside iron toroid magnets which provide a 1.8 T magnetic field, followed by two similar layers behind each toroid. Tracking in the muon system for $|\eta| < 1$ relies on 10 cm wide drift tubes [8], while 1 cm mini-drift tubes are used for $1 < |\eta| < 2$ [9].

The $H \rightarrow WW^{(*)}$ candidates are selected by single or di-lepton triggers using a three-level trigger system. The first trigger level uses hardware to select electron candidates based on energy deposition in the electromagnetic part of the calorimeter and selects muon candidates formed by hits in two layers of the muon scintillator system. Digital signal processors at the second trigger level form muon track candidate segments defined by hits in the muon drift chambers and scintillators. At the third level, software algorithms running on a computing farm and exploiting the full event information are used to make the final selection of events which are recorded for offline analysis.

In the offline analysis, electrons are identified as electromagnetic showers in the calorimeter. These showers are selected by comparing the longitudinal and transverse shower profiles to those expected of the electrons. The showers must be isolated, deposit most of their energy in the electromagnetic part of the calorimeter, and pass a likelihood criterion that includes a spatial track match and, in the CC region, an E/p requirement, where E is the energy of the calorimeter cluster and p is the momentum of the track. All electrons are required to be in the pseudorapidity range $|\eta| < 3.0$. The transverse momentum measurement of the electrons is based on calorimeter cell and track information.

Muon tracks are reconstructed from hits in the wire chambers and scintillators in the muon system and must match a track in the central tracker. To select isolated muons, the scalar sum of the transverse momentum of all tracks other than that of the muon in a cone of $\mathcal{R} = 0.5$ around the muon track must be less than 4 GeV, where $\mathcal{R} = \sqrt{(\Delta\phi)^2 + (\Delta\eta)^2}$ and ϕ is the azimuthal angle. Muon detection is performed over the full coverage of the muon system $|\eta| < 2.0$. Muons from cosmic rays are rejected by requiring a timing criterion on the hits in the scintillator layers as well as applying restrictions on the position of the muon track with respect to the primary vertex.

The decay of the two W bosons into electrons or muons results in three different final states $e^+e^- + X$ (ee channel), $e^\pm\mu^\mp + X$ ($e\mu$ channel) and $\mu^+\mu^- + X$ ($\mu\mu$ channel), each of which consists of two oppositely charged isolated leptons with high transverse momentum and large missing transverse energy, \cancel{E}_T , due to the undetected neutrinos. The selection criteria for each channel were chosen to minimize the cross section upper limit on Higgs production expected in the absence of signal. To take into account the signal kinematic characteristics that change with the Higgs boson mass, M_H , some selection cuts

are M_H dependent [10]. Six Higgs boson masses from 100 GeV to 200 GeV have been studied.

In all three channels, two leptons originating from the same vertex are required to be of opposite charge, and must have transverse momenta $p_T > 15$ GeV for the leading lepton and $p_T > 10$ GeV for the trailing one (Cut 1). Figure 1 shows the good agreement between data and Monte Carlo simulation (MC) in distributions of the azimuthal opening angle $\Delta\phi_{\ell\ell'}$ between the two leptons for the ee (a), the $\mu\mu$ (c) and the $e\mu$ channel (e) after applying the lepton transverse momentum cuts.

In all cases, the background is largely dominated by Z/γ^* production which is further suppressed by requiring $\cancel{E}_T > 20$ GeV in all three channels (Cut 2). Background events are also removed if the \cancel{E}_T has a large contribution from the mis-measurement of jet energy. The fluctuation in the measurement of jet energy in the transverse plane can be approximated by $\Delta E^{\text{jet}} \cdot \sin \theta^{\text{jet}}$ where ΔE^{jet} is proportional to $\sqrt{E^{\text{jet}}}$. The opening angle $\Delta\phi(\text{jet}, \cancel{E}_T)$ between this projected energy fluctuation and the missing transverse momentum provides a measure of the contribution of the jet to the missing transverse energy. The scaled missing transverse energy defined as

$$\cancel{E}_T^{\text{Sc}} = \frac{\cancel{E}_T}{\sqrt{\sum_{\text{jets}} (\Delta E^{\text{jet}} \cdot \sin \theta^{\text{jet}} \cdot \cos \Delta\phi(\text{jet}, \cancel{E}_T))^2}} \quad (1)$$

is required to be greater than 15 (Cut 3).

The charged lepton system and the neutrinos are emitted mostly back-to-back, so the invariant mass for the leptons from the Higgs decay is restricted to $M_H/2$. Thus, the invariant mass $m_{\ell\ell}$ is required to be $m_{\ell\ell} < M_H/2$ (Cut 4). In the ee channel the cut is altered to $m_{ee} < \min(80 \text{ GeV}, M_H/2)$. In the $\mu\mu$ channel a lower cut boundary with $m_{\mu\mu} > 20 \text{ GeV}$ is required to remove events from J/ψ , Υ and Z/γ^* production. The sum of the p_T of the leptons and \cancel{E}_T is required to be in the range $M_H/2 + 20 \text{ GeV} < p_T^{\ell_1} + p_T^{\ell_2} + \cancel{E}_T < M_H$ for the ee and $e\mu$ channel and $M_H/2 + 10 \text{ GeV} < p_T^{\ell_1} + p_T^{\ell_2} + \cancel{E}_T < M_H$ for the $\mu\mu$ channel (Cut 5). The transverse mass, defined

as $m_T^{\ell\ell'} = \sqrt{2p_T^{\ell\ell'} \cancel{E}_T (1 - \cos \Delta\phi(p_T^{\ell\ell'}, \cancel{E}_T))}$, with the di-lepton transverse momentum $p_T^{\ell\ell'}$, should be in the range $M_H/2 < m_T^{\ell\ell'} < M_H - 10 \text{ GeV}$ (Cut 6). The latter two cuts reject events from $W+\text{jet}/\gamma$ and WW production and further reduce backgrounds from Z/γ^* production. Finally, to suppress the background from $t\bar{t}$ production, the scalar sum of the transverse energies of all jets with $E_T^{\text{jet}} > 20 \text{ GeV}$ and $|\eta| < 2.5$, H_T , is required to be less than 100 GeV (Cut 7). Remaining Z boson and multi-jet events can be rejected with a cut on the opening angle, $\Delta\phi_{\ell\ell'} < 2.0$ (Cut 8), since most of the backgrounds exhibit a back-to-back topology. This is not the case for Higgs boson decays because of the spin correlations in the decay. Figure 1 shows the distributions of the azimuthal opening angle $\Delta\phi_{\ell\ell'}$ between the two leptons for the ee

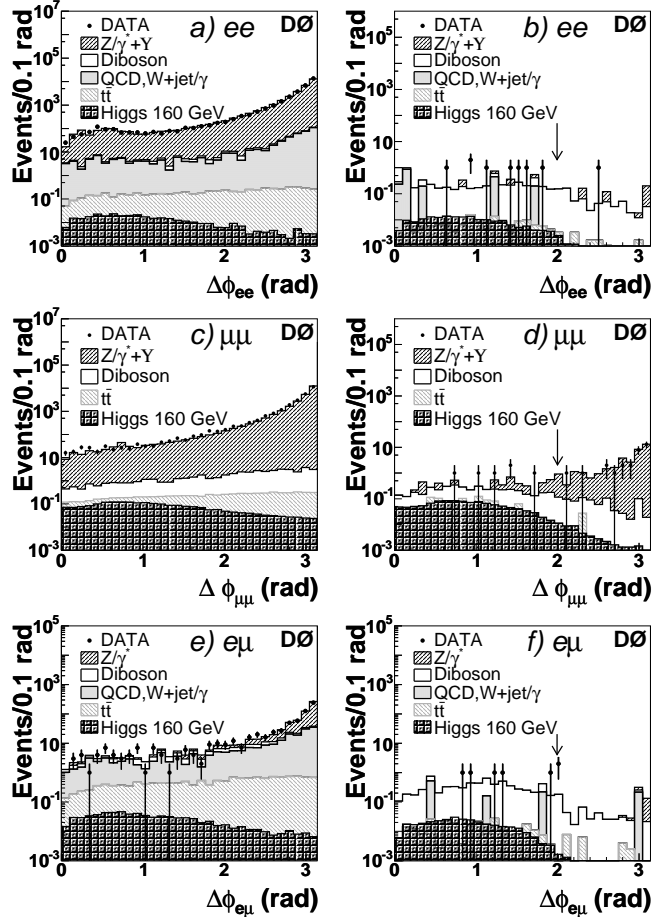


FIG. 1: Distribution of the opening angle $\Delta\phi_{\ell\ell'}$ after applying the initial transverse momentum cuts in the (a) ee , (c) $\mu\mu$ and (e) $e\mu$ channel. Figures (b), (d) and (f) show the $\Delta\phi_{\ell\ell'}$ distributions after the final selection except for the $\Delta\phi_{\ell\ell'}$ criterion for the ee , $\mu\mu$, and $e\mu$ channel, respectively. The arrows indicate the cut values. The QCD contribution is negligible in Figs. (c) and (d).

(b), the $\mu\mu$ (d) and the $e\mu$ channel (f) before applying the final cut on $\Delta\phi_{\ell\ell'}$.

To maximize the sensitivity, the selection in the $\mu\mu$ channel is slightly changed for Higgs boson masses $M_H = 140$ and 160 GeV. For a better Z/γ^* background suppression cuts 4, 5 and 6 are replaced by the following cuts: the invariant mass $m_{\mu\mu}$ should be in the range $20 \text{ GeV} < m_{\mu\mu} < 80 \text{ GeV}$ (Cut 4). Since the momentum resolution is degraded for high p_T tracks, an additional constrained fit is performed to reject events compatible with Z boson production (Cut 5). The sum of the muon transverse momenta and the missing transverse energy should be $p_T^{\mu 1} + p_T^{\mu 2} + \cancel{E}_T > 90 \text{ GeV}$ (Cut 6).

The efficiency for $H \rightarrow WW^{(*)} \rightarrow \ell\nu\ell'\nu'$ signal events to pass the acceptance and selection criteria is determined using the PYTHIA 6.2 [11] event generator followed by a detailed GEANT-based [12] simulation of the DØ detector. All trigger, reconstruction and identification effi-

TABLE I: Overall detection efficiencies (in %) for $H \rightarrow WW^{(*)} \rightarrow \ell\nu\ell'\nu'$ decays for the three channels after all cuts. Quoted are the overall uncertainties, combining statistical and systematic components in quadrature.

M_H (GeV)	ee	$e\mu$	$\mu\mu$
100	0.56 ± 0.05	1.02 ± 0.06	0.44 ± 0.03
120	1.18 ± 0.09	2.0 ± 0.1	1.02 ± 0.06
140	1.55 ± 0.08	2.9 ± 0.2	1.34 ± 0.08
160	2.1 ± 0.1	3.9 ± 0.2	2.0 ± 0.1
180	2.1 ± 0.1	3.9 ± 0.2	1.68 ± 0.09
200	1.57 ± 0.09	3.2 ± 0.1	1.53 ± 0.07

ciencies are derived from the data. The kinematic acceptance efficiency is derived from MC. The overall detection efficiencies range from $(0.44 \pm 0.03)\%$ to $(3.9 \pm 0.2)\%$ depending on the decay channel and M_H . Table I summarizes these efficiencies.

Using the NLO cross sections calculated with HIGLU [5] and HDECAY [4] and the branching ratio BR of 0.1068 ± 0.0012 for $W \rightarrow \ell\nu$ [13], the expected number of events for $H \rightarrow WW^{(*)}$ decays from all three channels is 0.68 ± 0.03 (syst) ± 0.04 (lum) events for a Higgs boson mass $M_H = 160$ GeV. The signal expectation for different Higgs masses M_H are given in Table II.

Background contributions from Z/γ^* , $W+\text{jet}/\gamma$, $t\bar{t}$, WW , WZ and ZZ events are estimated using the PYTHIA event generator normalized to their NLO cross sections [14]. In addition, $W+\text{jet}/\gamma$ contributions are verified using ALPGEN [15]. All events are processed through the full detector simulation. The background due to multi-jet production, when a jet is misidentified as an electron, is determined from the data using a sample of like-sign di-lepton events with inverted lepton quality cuts (called “QCD” in Fig. 1). A summary of the background contributions together with signal expectations and events observed in the data after the final selection is shown in Table II. There is good agreement between the number of events observed in the data and the various backgrounds in all three channels. The largest difference between the data and the background expectation, at $M_H = 120$ GeV, corresponds to a background probability of 6%. The $e\mu$ channel has both the highest signal efficiency and best signal-to-background ratio.

Various sources of systematic uncertainties that affect the background estimation and signal efficiencies have been studied. In these calculations, parameters are varied within $\pm 1\sigma$ of their nominal values, where σ is determined by the corresponding uncertainties. The trigger efficiency, electron and muon identification efficiencies, jet energy scale, electron and muon momentum resolution, parton distribution function uncertainty and cross section calculation of Z/γ^* , WW and $t\bar{t}$ events contribute to the systematic uncertainties. The total systematic uncertainties for the background estimate and signal effi-

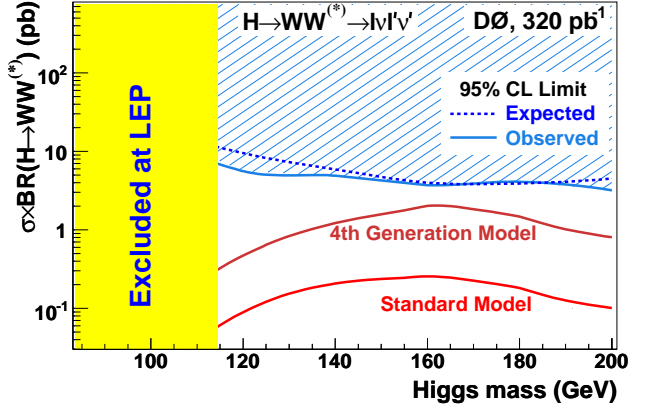


FIG. 2: Expected and observed upper limits on the cross section times branching ratio $\sigma \times BR(H \rightarrow WW^{(*)})$ at the 95% CL together with expectations from standard model Higgs boson production and an alternative model. The LEP limit on the standard model Higgs boson production is taken from [1] and the 4th generation model prediction is described in [6].

ciencies for the six Higgs boson masses are given in Table III. The largest contribution to the systematic uncertainty on the background for small Higgs boson masses comes from the jet energy scale due to the large $W+\text{jet}/\gamma$ background, whereas for high Higgs boson masses the W boson pair production cross section gives the largest systematic uncertainty. The uncertainty of the parton distribution function is the largest uncertainty of the signal efficiency. The uncertainty of the luminosity measurement is 6.5%.

Since the remaining candidate events after the selection are consistent with the background expectation, limits on the production cross section times branching ratio $\sigma \times BR(H \rightarrow WW^{(*)})$ are derived using a modified frequentist method described in Ref. [16]. It provides the confidence level for the background to represent the data, CL_B , and the confidence level for the sum of signal and background hypothesis CL_{S+B} . The 95% CL limit is obtained by requiring $CL_{S+B}/CL_B = 0.05$. The uncertainty on the background and the expected signal events were determined from the statistical and systematic uncertainties and luminosity uncertainty. Table IV shows the individual expected and observed upper limits on the cross section times branching ratio $\sigma \times BR(H \rightarrow WW^{(*)})$ for the combination of the three different decay channels for six different Higgs boson masses. The different values of the upper limits are due to different background expectations and signal efficiencies. The best limits are achieved for large Higgs masses since background expectations decrease while signal efficiencies increase.

Figure 2 shows the expected and observed cross section limits for $\sigma \times BR(H \rightarrow WW^{(*)})$ for the different Higgs boson masses compared with predictions from the SM and from an extension including a fourth fermion fam-

TABLE II: Number of signal and background events expected and number of events observed after all selections are applied. Only statistical uncertainties are given.

M_H (GeV)	100	120	140	160	180	200
$H \rightarrow WW^{(*)}$	0.007 ± 0.001	0.125 ± 0.002	0.398 ± 0.008	0.68 ± 0.01	0.463 ± 0.009	0.210 ± 0.004
Z/γ^*	7.9 ± 1.1	7.5 ± 1.0	3.8 ± 0.6	4.0 ± 0.7	6.6 ± 0.9	9.9 ± 1.1
Diboson	4.4 ± 0.2	8.1 ± 0.2	11.7 ± 0.3	12.3 ± 0.3	11.6 ± 0.3	9.6 ± 0.3
$t\bar{t}$	0.03 ± 0.01	0.11 ± 0.02	0.29 ± 0.02	0.47 ± 0.03	0.66 ± 0.05	0.72 ± 0.05
$W + \text{jet}/\gamma$	16.9 ± 2.2	14.2 ± 2.1	5.8 ± 1.2	2.8 ± 0.9	0.7 ± 0.5	0.7 ± 0.5
Multi-jet	0.6 ± 0.3	0.3 ± 0.1	0.2 ± 0.1	0.2 ± 0.1	0.3 ± 0.1	0.3 ± 0.1
Background sum	29.9 ± 2.5	30.1 ± 2.3	21.8 ± 1.4	19.7 ± 1.2	19.8 ± 1.1	21.2 ± 1.2
Data	27	21	20	19	19	14

TABLE III: Systematic uncertainties (in %) of the $H \rightarrow WW^{(*)}$ signal efficiencies and of the number of background events (BG), for the ee , $e\mu$ and $\mu\mu$ channels. Uncertainties exclude the uncertainty of the luminosity measurement.

M_H (GeV)	ee		$e\mu$		$\mu\mu$	
	Signal	BG	Signal	BG	Signal	BG
100	8.3	9.5	6.4	11.4	7.8	7.2
120	8.3	8.6	6.7	13.6	7.3	7.5
140	6.4	6.7	6.9	13.6	7.2	8.3
160	6.6	7.3	6.7	12.0	7.1	8.3
180	6.9	10.3	6.6	13.0	7.3	14.6
200	6.8	10.6	6.1	12.3	6.9	18.1

TABLE IV: Expected and observed upper limits at the 95% CL for the Higgs boson production cross section times branching ratio $\sigma \times BR(H \rightarrow WW^{(*)})$ for six values of M_H .

M_H (GeV)	100	120	140	160	180	200
Expected limits (pb)	20.3	9.5	5.9	4.0	3.9	4.5
Observed limits (pb)	18.5	5.6	4.9	3.7	4.1	3.2

ily [6]. With the current dataset, no region of the SM prediction can be excluded.

To conclude, we have searched for the Higgs boson in $H \rightarrow WW^{(*)} \rightarrow \ell\nu\ell'\nu'$ ($\ell, \ell' = e, \mu, \tau$) decays with e^+e^- , $e^\pm\mu^\mp$ or $\mu^+\mu^-$ final states in $p\bar{p}$ collisions at $\sqrt{s} = 1.96$ TeV. The data is consistent with the expectation from backgrounds. Since no excess has been observed, limits on the production cross section times branching ratio $\sigma \times BR(H \rightarrow WW^{(*)})$ have been derived.

We thank the staffs at Fermilab and collaborating institutions, and acknowledge support from the DOE and NSF (USA); CEA and CNRS/IN2P3 (France); FASI, Rosatom and RFBR (Russia); CAPES, CNPq, FAPERJ, FAPESP and FUNDUNESP (Brazil); DAE and DST (India); Colciencias (Colombia); CONACyT (Mexico); KRF (Korea); CONICET and UBACyT (Argentina);

FOM (The Netherlands); PPARC (United Kingdom); MSMT (Czech Republic); CRC Program, CFI, NSERC and WestGrid Project (Canada); BMBF and DFG (Germany); SFI (Ireland); Research Corporation, Alexander von Humboldt Foundation, and the Marie Curie Program.

[*] Visitor from University of Zurich, Zurich, Switzerland.

- [1] R. Barate *et al.*, Phys. Lett. **B** **565** (2003) 61.
- [2] The LEP Collaborations ALEPH, DELPHI, L3, OPAL, the LEP Electroweak Working Group, the SLD Electroweak and Heavy Flavour Groups, arXiv:hep-ex/0412015.
- [3] M. Carena *et al.*, arXiv:hep-ph/0010338.
- [4] A. Djouadi *et al.*, Comput. Phys. Commun. **108**, 56 (1998).
- [5] M. Spira, Report DESY T-95-05 (October 1995), arXiv:hep-ph/9510347.
- [6] E. Arik, O. Cakir, S. A. Cetin and S. Sultansoy, Phys. Rev. D **66**, 033003 (2002); O. Cakir and S. Sultansoy, Phys. Rev. D **65**, 013009 (2002).
- [7] DØ Collaboration, V. Abazov *et al.*, submitted to Nucl. Instrum. Methods A, arXiv:physics/0507191.
- [8] DØ Collaboration, S. Abachi *et al.*, Nucl. Instrum. Methods Phys. Res. A **338**, 185 (1994).
- [9] V. Abramov *et al.*, “The Muon System of the Run II DØ Detector”, arXiv:physics/0503151.
- [10] T. Han, A. S. Turcot and R. J. Zhang, Phys. Rev. D **59**, 093001 (1999).
- [11] T. Sjöstrand *et al.*, Comp. Phys. Comm. **135**, 238 (2001).
- [12] R. Brun and F. Carminati, CERN Program Library Long Writeup W5013, 1993 (unpublished).
- [13] Particle Data Group, S. Eidelman *et al.*, Phys. Lett. B **592**, 1 (2004).
- [14] V. M. Abazov *et al.*, Phys. Rev. Lett. **94**, 151801 (2005).
- [15] M.L. Mangano *et al.*, J. High Energy Phys. **0307**, 001 (2003).
- [16] T. Junk, Nucl. Instrum. and Methods A **434**, 435 (1999).